

Automatic coronary lumen segmentation with partial volume modeling improves lesions' hemodynamic significance assessment

M. Freiman^a, Y. Lamash^a, G. Gilboa^b, H. Nickisch^c, S. Prevrhal^c, H. Schmitt^c, M. Vembar^d
and L. Goshen^a

^aGRAD, CT, Philips Healthcare, Haifa, Israel;

^bFaculty of Electrical Engineering, Technion, Haifa, Israel;

^cPhilips Research, Hamburg, Germany;

^dClinical Science, CT, Philips Healthcare, Cleveland, Ohio, USA

ABSTRACT

The determination of hemodynamic significance of coronary artery lesions from cardiac computed tomography angiography (CCTA) based on blood flow simulations has the potential to improve CCTA's specificity, thus resulting in improved clinical decision making. Accurate coronary lumen segmentation required for flow simulation is challenging due to several factors. Specifically, the partial-volume effect (PVE) in small-diameter lumina may result in overestimation of the lumen diameter that can lead to an erroneous hemodynamic significance assessment. In this work, we present a coronary artery segmentation algorithm tailored specifically for flow simulations by accounting for the PVE. Our algorithm detects lumen regions that may be subject to the PVE by analyzing the intensity values along the coronary centerline and integrates this information into a machine-learning based graph min-cut segmentation framework to obtain accurate coronary lumen segmentations. We demonstrate the improvement in hemodynamic significance assessment achieved by accounting for the PVE in the automatic segmentation of 91 coronary artery lesions from 85 patients. We compare hemodynamic significance assessments by means of fractional flow reserve (FFR) resulting from simulations on 3D models generated by our segmentation algorithm with and without accounting for the PVE. By accounting for the PVE we improved the area under the ROC curve for detecting hemodynamically significant CAD by 29% (N=91, 0.85 vs. 0.66, $p < 0.05$, Delong's test) with invasive FFR threshold of 0.8 as the reference standard. Our algorithm has the potential to facilitate non-invasive hemodynamic significance assessment of coronary lesions.

Keywords: Coronary CT Angiography, Coronary Artery Disease, Segmentation, Fractional Flow Reserve Simulation, Partial Volume effect

1. INTRODUCTION

Coronary artery disease (CAD) is the single largest cause of death worldwide, causing 7,249,000 deaths in 2008, 12.7% of total global mortality.¹ Cardiac Computed Tomography Angiography (CCTA) is a rapidly evolving technique for the non-invasive evaluation of coronary artery disease (CAD). The high negative predictive value in CAD detection positions CCTA as a preferred non-invasive technique to rule out CAD in symptomatic patients with low to intermediate pre-test probability of disease.² However, CCTA is limited in assessing hemodynamic significance of coronary lesions.³ Recent studies suggest that coronary lesions' hemodynamic significance assessment from CCTA by means of Fractional Flow Reserve (FFR, i.e. the ratio between the pressure after a lesion and the normal pressure) based on flow simulation, can improve the specificity of CCTA.⁴⁻⁸

Assessing hemodynamic significance from CCTA requires accurate segmentation of the coronaries to generate the three-dimensional model for flow simulations. For example, Coenen et al report that the time required for semi-automatic coronary segmentation for flow simulation varies depending on the extent of atherosclerotic disease, with a range of 30-120 minutes per patient.⁵ This time-consuming semi-automatic segmentation step may therefore impede the routine clinical utilization of flow simulation as part of the CCTA exam.

Vessel segmentation in general,⁹ and coronary segmentation from CCTA in particular,¹⁰ has been a major topic of interest in the past few years. Lugauer et al^{11,12} obtained the best reported results on the MICCAI

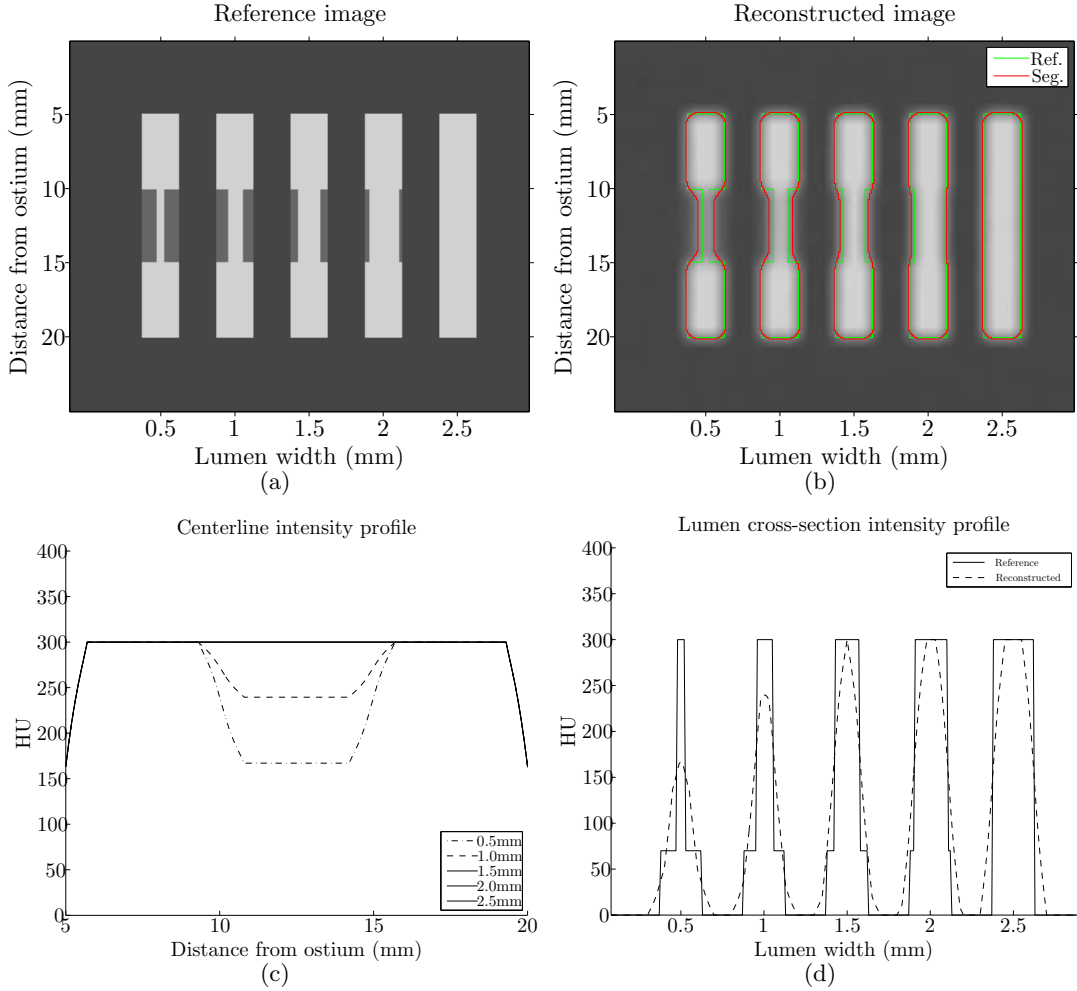


Figure 1. Illustration of the partial volume effect. (a) The reference image, including ideal vessel profiles with varying stenosis percentage due to the presence of soft-plaque. (b) The reconstructed image, with the reference segmentation in green and full-width half maximum (FWHM) segmentation in red). Note the over-estimation of the lumen diameter due to the partial volume effect. (c) The vessel intensity profile. (d) the vessels cross-sectional intensity profile. The HU reduction in the centerline intensity profile can be used to determine locations that affected by partial volume effect.

2012 challenge database¹⁰ by using a learning-based boundary detection model, combined with a graph min-cut based optimal surface generation. However, the evaluation was focused on anatomical agreement between the automatic and manual segmentations rather than on the evaluation of their impact on coronary lesion hemodynamic significance assessment.

Most coronary segmentation algorithms in the literature address the challenge of accurately separating between the coronary lumen and the accumulated plaque inside the vessel. However, the partial-volume effect (PVE) due to the finite resolution of imaging scanners and blurring involved in the reconstruction which are integrated into the overall system Point Spread Function (PSF) may lead to an overestimation of lumen area in vessels with small lumen diameter,^{13,14} and as a result may cause underestimation of the lesion's hemodynamic significance. Fig. 1 illustrates this effect on 2D vessel profiles with varying stenosis percentage due to the presence of non-calcified plaque.

In this work we present a coronary segmentation algorithm that accounts for the PVE in the coronary arteries. Our approach first analyzes the intensity values along the coronary centerline to detect regions with small diameter lumen that may be overestimated due to the PVE. Then, the underlying lumen radius is recovered and integrated into a machine-learning based graph-cut segmentation framework¹⁵ to obtain the final segmentation.

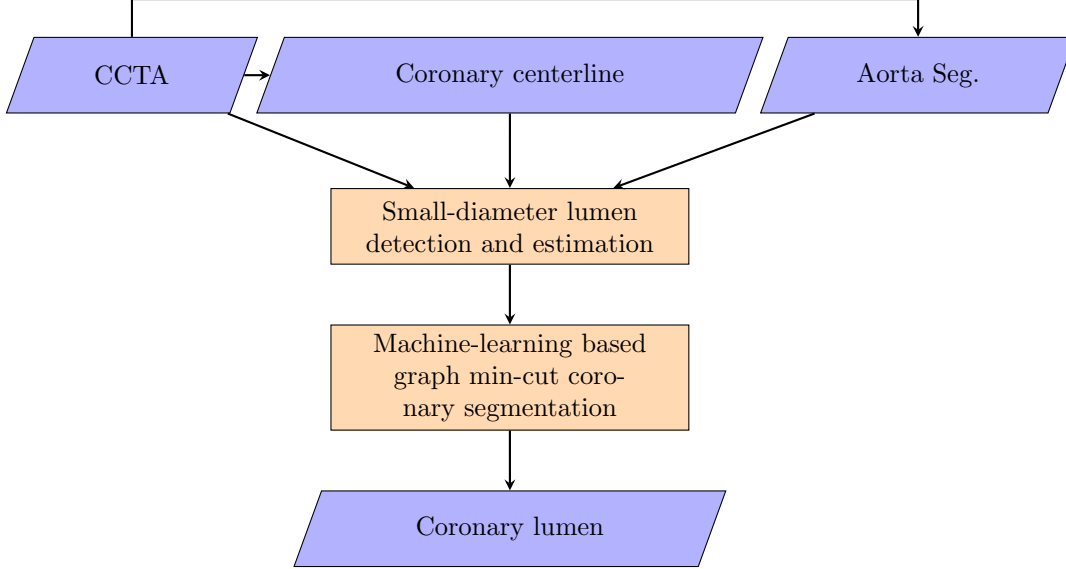


Figure 2. Coronary lumen segmentation algorithm flowchart.

We evaluated the impact of accounting for the PVE on CCTA hemodynamic significance assessment in 91 lesions from 85 patients. We compared the area under the ROC curve for detecting hemodynamic significant CAD by means of fractional flow reserve (FFR) simulated using 3D models generated by our automatic segmentation algorithm with and without accounting for the PVE.

2. METHOD

The input to our coronary lumen segmentation algorithm includes the CCTA volume, the coronary-artery centerlines and the segmentation of the aortic root. The coronary artery centerlines and the aorta segmentation can be computed automatically using existing methods^{16–20} and may be adjusted manually to account for algorithm errors.

The coronary lumen segmentation algorithm consists of the following steps. 1) Analysis of the intensity profile along the coronary centerline to detect regions with small diameter lumen that may be overestimated due to the PVE, 2) Estimating underlying lumen radius, and 3) machine-learning based graph-cut segmentation¹⁵ to obtain final segmentation. Fig. 2 presents the flowchart of the proposed algorithm. We describe each step in detail next.

2.1 Small-diameter lumen detection and estimation

Given a cardiac CT angiography volume (I) with a coronary centerline (C), our goal is to determine locations along the coronary centerline that might be subject to the PVE. Our approach relies upon a two-phase robust intensity profile model fitting with outlier detection. First, we model the expected intensity profile along the coronary centerline as a quadratic polynomial function $I_p(C)$. We fit the model $I_p(C)$ to the intensity profile along the centerline $I(C)$ using a least-squares fitting.

$$\widehat{I_p(C)} = \operatorname{argmin}_{I_p(C)} \sum_{c \in C} \left(I(c) - I_p(c) \right)^2 \quad (1)$$

We identify potential outliers in the measured intensity profile by applying the Student’s t-test to determine points along the centerline that are statistically significantly different (i.e. $p < 0.05$) from the estimated model. We obtain a robust centerline intensity profile model by excluding these outliers from the centerline, i.e. $C_{clean} = C \setminus C_{outliers}$ and repeating the fitting process with C_{clean} instead of C . Finally, we identify regions with reduced vessel

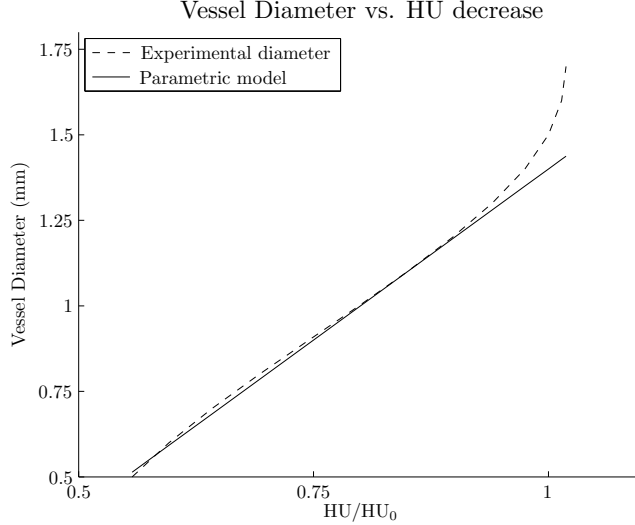


Figure 3. Experimental measurement of the percentage HU reduction as a function of the coronary diameter along with the fitted model (Eq. 3) where HU is the measured HU at the vessel centerline and HU_0 is the expected HU at the location without the PVE.

diameter that may be affected by the PVE by determining points along the centerline with intensity values that are more than 2 standard deviations below the intensity expected by the model and without the presence of calcified plaque:

$$\mathbb{1}_{pv}(c) = \begin{cases} 1, & I(c) > (I_p(c) - 2\sigma_{I_c}) \\ 0, & I(c) \leq (I_p(c) - 2\sigma_{I_c}) \end{cases} \quad (2)$$

where σ_{I_c} is the standard deviation over the differences between the intensity profile along the centerline $I(C)$ and the fitted intensity model $I_p(C)$. Inspired by Sato et al,¹⁴ we model the radius of the coronary lumen at centerline location c as a function of the percentage of the lumen intensity decrease:

$$r(c) = 0.5 \left(\alpha \left(1 - \frac{I(c)}{I_p(c)} \right) + \beta \right) \quad (3)$$

where $r(c)$ is units of mm. We determine the model coefficients values α , β by simulating the impact of the approximated system PSF on ideal vessel profiles with varying diameter and fitting the model to the observed data. Based on our simulations we set the values of α and β to -2.0mm and 1.4mm respectively. Note that this function is valid for diameter estimation where the observed intensity ($I(c)$) is smaller than the expected intensity ($I_p(c)$) only. Fig. 3 presents the experimental measurement of the percentage HU reduction as a function of the coronary diameter along with the fitted model (Eq. 3) used in our method. Fig. 4 depicts a representative example of a coronary straight multi-planar reconstructed (MPR) image with small lumen diameter along with its centerline intensity profile and the detected small lumen diameter region.

2.2 Machine-learning based graph min-cut coronary segmentation

We first transform each coronary artery in the original 3D CCTA volume into a cylindrical coordinate system^{11,12} where warped volume is expressed with the coordinate i representing the index of the cross-sectional plane, and θ, r representing the angle and the radial distance determining a point in the cross-sectional plane. We then employ the graph min-cut segmentation framework¹⁵ to find the optimal surface separating the lumen from the background. Formally, we minimize the following energy:

$$E(X) = \sum_{p \in P} \Psi_p(x_p) + \lambda \sum_{p, q \in E} \Psi_{p, q}(x_p, x_q) \quad (4)$$

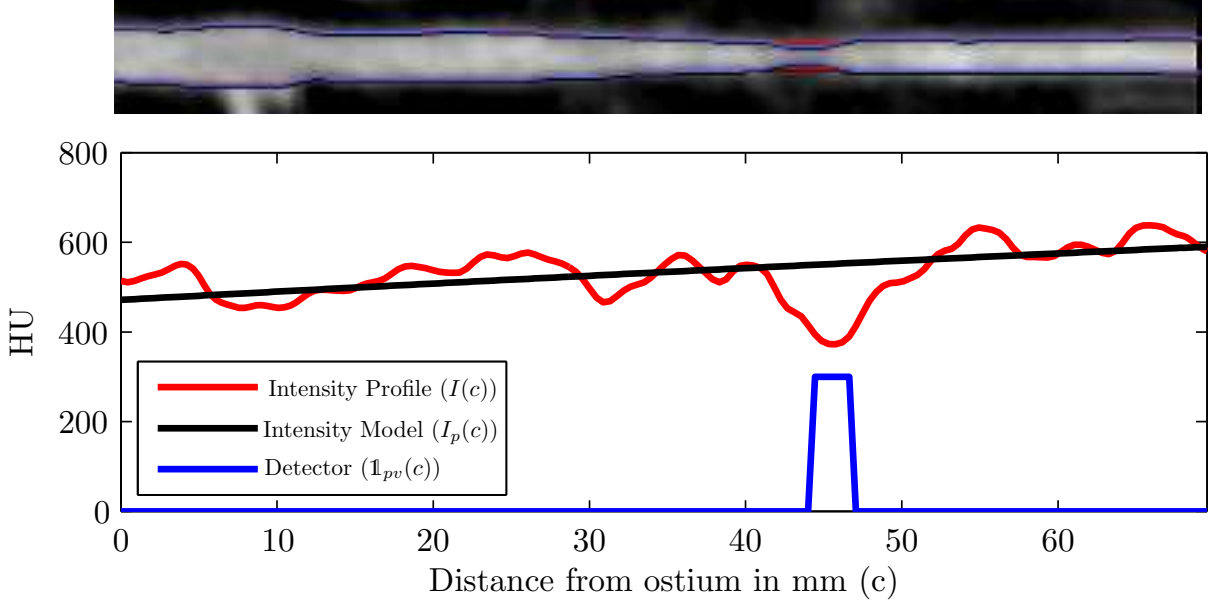


Figure 4. A representative example of a coronary straight multi-planar reconstructed image with small diameter lumen (top) along with its centerline intensity profile and the small diameter lumen region as detected by our method (bottom). Segmentation results are depicted on the top image in red for automatic graph min-cut segmentation without accounting for the PVE and in blue for the proposed algorithm.

where P is the set of sampled points, x_p is a vertex in the graph representing the point $(i^{x_p}, \theta^{x_p}, r^{x_p})$ sampled from the original CCTA volume, $\Psi_p(x_p)$ represents the likelihood of the vertex to belong to the lumen or background classes, p, q are neighboring points according to the employed neighboring system E , and $\Psi_{p,q}(x_p, x_q)$ is a regularization term penalizing for neighboring vertices belonging to different classes.

We calculate the likelihood of each vertex x_p to belong to the coronary lumen using a supervised machine-learning approach as follows. Assuming that a training database consists of rays sampled from cardiac CTA data along with matched binary rays representing the manual segmentation, we calculate the probability of x_p of belonging to the lumen using a kernel density estimation approach:

$$\Pr_d(x_p \in \text{Lumen}) = \frac{\sum_{k=1}^K w(I(i^{x_p}, \theta^{x_p}, R), I'(i^k, \theta^k, R)) \cdot \delta(x_p, S(i^k, \theta^k, R))}{\sum_{k=1}^K w(I(i, \theta^{x_p}, R^{x_p}), I'(i^k, \theta^k, R))} \quad (5)$$

where R is a set of radial distances, $I(i^{x_p}, \theta^{x_p}, R)$ is the sampled ray that include the point x_p in the new volume, $I'(i^k, \theta^k, R)$ is the ray from the training set, $\delta(x_p, I'(i^k, \theta^k, R))$ is an indicator function that indicates whether the point x_p is labeled with 1 on the binary ray $S(i^k, \theta^k, R)$ corresponding to the $I'(i^k, \theta^k, R)$ ray in the training data, K is the number of closest rays to be used, and $w(I(i^{x_p}, \theta^{x_p}, R), I'(i^k, \theta^k, R))$ is a weighting function that is used to weight the contribution of each training ray according to its distance from the test ray:

$$w(I(i^{x_p}, \theta^{x_p}, R), I'(i^k, \theta^k, R)) = \exp\left(-\lambda \|I(i^{x_p}, \theta^{x_p}, R) - I'(i^k, \theta^k, R)\|_2^2\right) \quad (6)$$

Next, for rays that belong to planes that were identified with potential small lumen diameter, we adjust the probability of points along the ray calculated at Eq. 5 to reflect the estimated radius, calculated as described in Sec. 2.1.

$$\Pr_{pv}(x_p \in \text{Lumen}) = \begin{cases} 0, & r^{x_p} \geq r' \\ 1, & r^{x_p} \leq r' \end{cases} \quad (7)$$

where r^{x_p} is the radial distance of the point x_p and r' is the estimated radius at the cross section i^{x_p} calculated as described in Sec. 2.1.

Next, we combined the two probabilities together:

$$\Pr(x_p \in \text{Lumen}) = \begin{cases} \Pr_d(x_p), & \mathbb{1}_{pv}(c(x_p)) = 0 \\ \Pr_{pv}(x_p), & \mathbb{1}_{pv}(c(x_p)) = 1 \end{cases} \quad (8)$$

where $c(x_p)$ is the centerline location that the sampling point x_p belongs to. We also adjust the probability of vertices that represent calcified plaque determined by HU above a fixed threshold to have high background probability value.

Finally we assign:

$$\Psi_p(x_p) = -\log \Pr(x_p \in \text{Lumen}) \quad (9)$$

To ensure surface smoothness we employ a standard L2 intensity difference regularization:²¹

$$\Psi_{p,q}(x_p, x_q) = \exp\left(-\frac{(I(x_p) - I(x_q))^2}{\sigma_c(x_p)}\right) \cdot \exp(-d(x_p, x_q)^2) \quad (10)$$

where $d(x_p, x_q)$ is the spatial distance between the vertices and $\sigma_c(x_p)$ is the standard deviation of the intensity in the cross section that x_p located on. We finally find the globally optimal lumen surface by calculating the minimal cut of the graph.

3. EXPERIMENTAL RESULTS

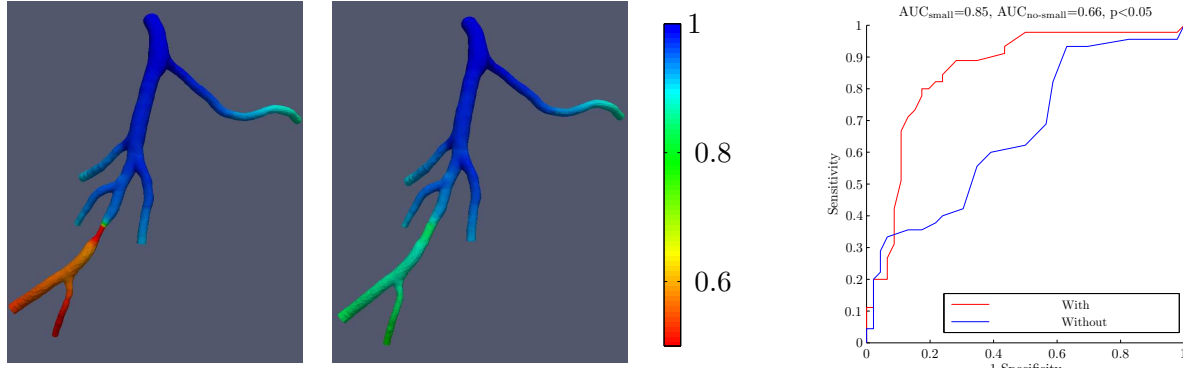
We implemented our main algorithm in MATLAB[®]. We used the graph min-cut solver of Boykov et al,¹⁵ and an accelerated approximated k nearest neighbor search.²² We experimentally set the value of the regularization term λ in Eq. 4 to 1.75 and K in Eq. 5 to 100. The average running time to segment the entire coronary tree lumen for each patient was ~ 1.5 minute. As boundary conditions for flow simulation we employed an ostial pressure of $\hat{p} = 100$ mmHg and outlet resistances R_i scaling with the outlet diameter d_i according to $R_i \propto d_i^{-1/3}$ ²³ for both left/right coronary trees independently.

We evaluated the improvement achieved by accounting for the PVE in the automatic segmentation on the hemodynamic significance assessment of coronary lesions on a database of 85 subjects with 91 lesions. Each subject data contains coronary centerlines annotated by an expert in cardiac imaging and invasive fractional flow reserve (FFR, i.e. the pressure distal to the lesion divided by the normal pressure) measurements. We generated 3D models of the coronary tree using our algorithm with and without accounting for the PVE in a leave-one-out fashion, in which the segmented case is excluded from the training database. We estimated the hemodynamic significance of each lesion by using the Netgen software library (<http://sourceforge.net/projects/netgen-mesher/>) to generate 3D patient-specific finite elements model of the coronary, and the OpenFoam software library(<http://www.openfoam.org/>) to determine the pressure along the coronary artery by solving the corresponding Navier-Stokes equations. Fig. 5 shows an example of the assessment of hemodynamic significance of a coronary lesion via a color-gradient representation using models generated with (a) and without (b) accounting for partial volume effect in the automatic segmentation.

We assessed the performance of simulated FFR measurements based on automatically generated coronary 3D models in detecting significant CAD with invasive FFR measurement threshold of 0.8 as the reference standard using Receiver Operating characteristic (ROC) analysis. Fig. 5(c) presents the ROC curves of the detection performance for the models generated with (red) and without (blue) accounting for the PVE. Accounting for the PVE in the automatic segmentation significantly improved the detection performance by means of area under the ROC curve (AUC) by 29% (N=91, 0.85 vs. 0.66, $p < 0.05$, Delong's test²⁴), with invasive FFR threshold of 0.8 as a reference.

4. CONCLUSION

Computational fluid dynamics techniques were proposed to assess the hemodynamic significance of coronary lesions with the overall goal of improving CCTA sensitivity to hemodynamic significant lesions in coronary artery disease. However, accurate 3D lumen segmentation required for flow simulation is challenging due to the



(a) With accounting for the PVE (b) Without accounting for the PVE (c) ROC analysis

Figure 5. (a-b) A representative example of hemodynamic significance assessment obtained with our automatic segmentation results with (a), and without (b) accounting for the PVE. (c) ROC analysis of hemodynamic significance assessment based on automatic segmentation with (red) and without (blue) accounting for the PVE, with invasive FFR threshold of 0.8 as the reference.

partial-volume effect which may result in overestimate of the lumina radius and therefore may result in erroneous estimation of hemodynamic significance of coronary lesions. In this work we have presented an algorithm for coronary segmentation that accounts for the partial volume effect. Our algorithm detects locations which might be subject to partial volume effect by analyzing the intensity values along the coronary centerline. Then, our algorithm incorporates this information into a machine-learning based graph min-cut segmentation framework to obtain final 3D model of the coronary artery. We demonstrated a significant improvement in non-invasive hemodynamic significance assessment of coronary lesions by using the proposed algorithm.

REFERENCES

- [1] Finegold, J. et al., “Mortality from ischaemic heart disease by country, region, and age: Statistics from World Health Organisation and United Nations,” *Int J Cardiol* **168**(2), 934–945 (2013).
- [2] Arbab-Zadeh, A. et al., “Quantification of coronary arterial stenoses by multidetector CT angiography in comparison with conventional angiography methods, caveats, and implications,” *JACC Cardiovasc Imaging* **4**(2), 191–202 (2011).
- [3] Meijboom, W. et al., “Comprehensive assessment of coronary artery stenoses: computed tomography coronary angiography versus conventional coronary angiography and correlation with fractional flow reserve in patients with stable angina,” *J Am Coll Cardiol* **52**(8), 636–643 (2008).
- [4] Nørgaard, B. et al., “Diagnostic performance of noninvasive fractional flow reserve derived from coronary computed tomography angiography in suspected coronary artery disease: the NXT trial (Analysis of Coronary Blood Flow Using CT Angiography: Next Steps),” *J Am Coll Cardiol* **63**(12), 1145–1155 (2014).
- [5] Coenen, A. et al., “Fractional Flow Reserve Computed from Noninvasive CT Angiography Data: Diagnostic Performance of an On-Site Clinician-operated Computational Fluid Dynamics Algorithm,” *Radiology* **274**(3), 674–683 (2015).
- [6] Min, J. et al., “Noninvasive Fractional Flow Reserve Derived From Coronary CT Angiography: Clinical Data and Scientific Principles,” *JACC Cardiovasc Imaging* **8**(10), 1209–1222 (2015).
- [7] Gonzalez, J. et al., “Meta-Analysis of Diagnostic Performance of Coronary Computed Tomography Angiography, Computed Tomography Perfusion, and Computed Tomography-Fractional Flow Reserve in Functional Myocardial Ischemia Assessment Versus Invasive Fractional Flow Reserve,” *Am J Cardiol* **116**(9), 1469–1478 (2015).
- [8] Nickisch, H. et al., “Learning Patient-Specific Lumped Models for Interactive Coronary Blood Flow Simulations,” in *[Medical Image Computing and Computer-Assisted Intervention – MICCAI 2015]*, Navab, N., Hornegger, J., Wells, W. M., and Frangi, A. F., eds., *Lecture Notes in Computer Science* **9350**, 433–441, Springer International Publishing (2015).

- [9] Lesage, D. et al., “A review of 3D vessel lumen segmentation techniques: models, features and extraction schemes,” *Med Image Anal* **13**(6), 819–845 (2009).
- [10] Kirişli, H. et al., “Standardized evaluation framework for evaluating coronary artery stenosis detection, stenosis quantification and lumen segmentation algorithms in computed tomography angiography,” *Med Image Anal* **17**(8), 859–876 (2013).
- [11] Lugauer, F. et al., “Precise Lumen Segmentation in Coronary Computed Tomography Angiography,” in [*Proc. of MICCAI 2014 Workshop on Medical Computer Vision: Algorithms for Big Data*], Menze, B. et al., eds., *Lecture Notes in Computer Science* **8848**, 137–147, Springer (2014).
- [12] Lugauer, F., Zhang, J., Zheng, Y., Hornegger, J., and Kelm, B. M., “Improving accuracy in coronary lumen segmentation via explicit calcium exclusion, learning-based ray detection and surface optimization,” in [*SPIE Medical Imaging*], 90343U–90343U, International Society for Optics and Photonics (2014).
- [13] Prevrhal, S. et al., “Accuracy of CT-based thickness measurement of thin structures: modeling of limited spatial resolution in all three dimensions,” *Med Phys* **30**(1), 1–8 (2003).
- [14] Sato, Y. et al., “Accurate Quantification of Small-Diameter Tubular Structures in Isotropic CT Volume Data Based on Multiscale Line Filter Responses,” in [*Medical Image Computing and Computer-Assisted Intervention MICCAI 2004*], Barillot, C., Haynor, D., and Hellier, P., eds., *Lecture Notes in Computer Science* **3216**, 508–515, Springer (2004).
- [15] Boykov, Y. et al., “Graph Cuts and Efficient N-D Image Segmentation,” *Int. J Computer Vision (IJCV)* **70**(2), 109–131 (2006).
- [16] Schaap, M. et al., “Standardized Evaluation Methodology and Reference Database for Evaluating Coronary Artery Centerline Extraction Algorithms,” *Med Image Anal* **13**(5), 701–714 (2009).
- [17] Zheng, Y., Tek, H., and Funka-Lea, G., “Robust and Accurate Coronary Artery Centerline Extraction in CTA by Combining Model-Driven and Data-Driven Approaches,” in [*Medical Image Computing and Computer-Assisted Intervention MICCAI 2013*], Mori, K., Sakuma, I., Sato, Y., Barillot, C., and Navab, N., eds., *Lecture Notes in Computer Science* **8151**, 74–81, Springer Berlin Heidelberg (2013).
- [18] Freiman, M. et al., “Carotid vasculature modeling from patient CT angiography studies for interventional procedures simulation,” *Int J Comput Assist Radiol Surg* **7**(5), 799–812 (2012).
- [19] Ecabert, O. et al., “Segmentation of the heart and great vessels in CT images using a model-based adaptation framework,” *Med Image Anal* **15**(6), 863–876 (2011).
- [20] Ecabert, O. et al., “Automatic model-based segmentation of the heart in CT images,” *IEEE Trans Med Imaging* **27**(9), 1189–1201 (2008).
- [21] Boykov, Y. Y. and Jolly, M.-P., “Interactive graph cuts for optimal boundary & region segmentation of objects in ND images,” in [*Proceedings. 8th IEEE International Conference on Computer Vision, 2001. ICCV 2001.*], **1**, 105–112, IEEE (2001).
- [22] Muja, M. et al., “Fast approximate nearest neighbors with automatic algorithm configuration,” in [*International Conference on Computer Vision Theory and Application VISSAPP’09*], 331–340, INSTICC Press (2009).
- [23] Huo, Y. and Kassab, G. S., “Intraspecific scaling laws of vascular trees,” *J R Soc Interface* **9**(66), 190–200 (2012).
- [24] DeLong, E. R. et al., “Comparing the areas under two or more correlated receiver operating characteristic curves: a nonparametric approach,” *Biometrics* , 837–845 (1988).